JCI insight

RESEARCH ARTICLE

Disease-modifying effects of orally bioavailable NF-κB inhibitors in dystrophin-deficient muscle

David W. Hammers,[1,2,3,4] Margaret M. Sleeper,[4,5,6] Sean C. Forbes,[4,7] Cora C. Coker,[3,4] Michael R. Jirousek,[8] Michael Zimmer,[8] Glenn A. Walter,[4,9] and H. Lee Sweeney[1,3,4]

[1]Department of Physiology and [2]Pennsylvania Muscle Institute, University of Pennsylvania Perelman School of Medicine, Philadelphia, Pennsylvania, USA. [3]Department of Pharmacology and Therapeutics, [4]Myology Institute and [9]Department of Physiology and Functional Genomics, University of Florida College of Medicine, Gainesville, Florida, USA. [5]Department of Clinical Studies, University of Pennsylvania School of Veterinary Medicine, Philadelphia, Pennsylvania, USA. [6]Department of Small Animal Clinical Sciences, University of Florida College of Veterinary Medicine, [7]Department of Physical Therapy, University of Florida, Gainesville, Florida, USA. [8]Catabasis Pharmaceuticals, Inc., Cambridge, Massachusetts, USA.

Duchenne muscular dystrophy (DMD) is a devastating muscle disease characterized by progressive muscle deterioration and replacement with an aberrant fatty, fibrous matrix. Chronic upregulation of nuclear factor κB (NF-κB) is implicated as a driver of the dystrophic pathogenesis. Herein, 2 members of a novel class of NF-κB inhibitors, edasalonexent (formerly CAT-1004) and CAT-1041, were evaluated in both *mdx* mouse and golden retriever muscular dystrophy (GRMD) dog models of DMD. These orally bioavailable compounds consist of a polyunsaturated fatty acid conjugated to salicylic acid and potently suppress the pathogenic NF-κB subunit p65/RelA in vitro. In vivo, CAT-1041 effectively improved the phenotype of *mdx* mice undergoing voluntary wheel running, in terms of activity, muscle mass and function, damage, inflammation, fibrosis, and cardiac pathology. We identified significant increases in dysferlin as a possible contributor to the protective effect of CAT-1041 to sarcolemmal damage. Furthermore, CAT-1041 improved the more severe GRMD phenotype in a canine case study, where muscle mass and diaphragm function were maintained in a treated GRMD dog. These results demonstrate that NF-κB modulation by edasalonexent and CAT-1041 is effective in ameliorating the dystrophic process and these compounds are candidates for new treatments for DMD patients.

Introduction

Duchenne muscular dystrophy (DMD) is a lethal X-linked disease, affecting 1 in 3,500 males, caused by loss of the sarcolemma-stabilizing protein, dystrophin (1, 2). The chronic inflammation caused by constant muscular degeneration in DMD is heavily implicated in the progressive replacement of functional muscle with fibrotic fatty tissue, as the constant muscle damage causes discoordinate mixing of proinflammatory and antiinflammatory signals.

Nuclear factor κB (NF-κB) is an evolutionarily conserved, polymorphic, and pleiotropic system of transcriptional regulation designed to respond to cellular stress in a rapid and transient manner, promoting cell survival. Canonical NF-κB (cNF-κB) signaling involves activation of p65-p50 heterodimers by IKK-mediated release from IκB (3). During this process, IκB is phosphorylated by the IKK complex and is rapidly degraded by the proteasome to release the p65-p50 heterodimer (3), allowing nuclear translocation and subsequent transcriptional activation of NF-κB–responsive genes. Typical cNF-κB–induced genes include inflammatory cytokines and cNF-κB feedback regulatory products to counter p65-dependent activity (4, 5). An IκB-independent, alternative NF-κB pathway (altNF-κB) exists that involves the activation of RelB-p52 heterodimers by IKKα-induced proteolytic cleavage of p100 into p52 (3). Additionally, phosphorylation of a pool of IκB-independent p65 on Ser536 has been reported to result in p65-p65 homodimer formation and activation of genes distinct from cNF-κB activation (6); however, recent evidence suggests this modification serves as a brake on p65-dependent transcription (7).

Though these pathways are essential to organism survival and adaptation, chronic activation of the NF-κB system results in uncontrolled inflammatory pathology. Such is the case in dystrophin-deficient

Conflict of interest: MRJ and MZ were employees and shareholders of Catabasis Pharmaceuticals, Inc. at the time of this study. The other authors have declared that no conflict of interest exists.

Submitted: August 26, 2016
Accepted: November 8, 2016
Published: December 22, 2016

Reference information:
JCI Insight. 2016;1(21):e90341.
doi:10.1172/jci.insight.90341.

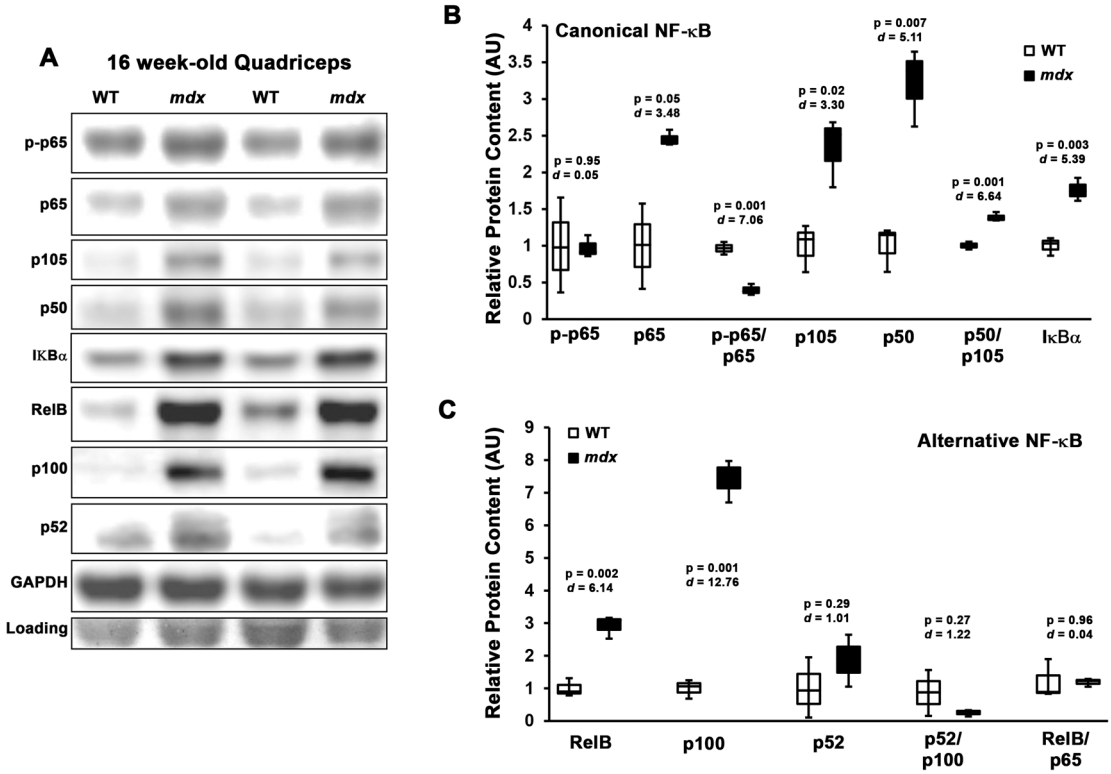

Figure 1. NF-κB components are elevated in stabilized *mdx* muscle. (**A**) Representative immunoblot images of 16-week-old WT (n = 3) and *mdx* (n = 3) quadriceps with accompanying quantifications for (**B**) canonical and (**C**) alternative NF-κB component protein levels. Protein levels were normalized to Ponceau red–visualized loading (Loading) and quantified relative to WT values. Data are displayed as box-and-whisker plots, indicating first and third quartiles, median, minimum, and maximum values, and were analyzed using 2-tailed Welch's t test with effect size displayed as Cohen's d.

muscle, where chronic activation of cNF-κB occurs in the muscle of dystrophic mice (8, 9) and DMD patients (10, 11). In agreement with NF-κB–dependent pathogenesis, genetic haploinsufficiency experiments in the *mdx* mouse model of DMD have confirmed that reduction of p65, but not p50, improves the dystrophic phenotype and affects both the muscle fibers and immune infiltrate (8). Accordingly, inhibition of NF-κB in dystrophic muscle via gene therapy with a dominant-negative IKKα or IKKβ (12) or peptide-based IKKγ inhibitors (8, 13, 14) has impressive therapeutic potential; however, both of these strategies are problematic for immediate translation.

The current report details the investigation of a novel class of orally bioavailable NF-κB inhibitors for the treatment of dystrophic muscle. These compounds are composed of a polyunsaturated fatty acid (PUFA) and salicylic acid, molecules individually known to inhibit the activation of cNF-κB (15, 16), conjugated together by a linker that is only susceptible to hydrolysis by intracellular fatty acid hydrolase (17). Herein, we present data that demonstrate that 2 compounds of this class (edasalonexent [formerly CAT-1004] and CAT-1041) potently inhibit cNF-κB activation in vitro, and that long-term treatment improves the phenotype of both the *mdx* mouse and golden retriever muscular dystrophy (GRMD) dog models of DMD. These results suggest that this class of NF-κB inhibitors can serve as an effective treatment to slow disease progression in DMD patients.

Results

We first verified the increases in NF-κB component proteins in our mouse model of dystrophic muscle by comparing 4-month-old WT and *mdx* mouse quadriceps for both cNF-κB and altNF-κB components (Figure 1, A–C). As expected, every measured component of the cNF-κB pathway, including p65, p105, p50, and IκB, was significantly elevated in *mdx* muscle (Figure 1B). Absolute phosphorylation of p65 on Ser536 is unchanged in dystrophic muscle; thus, the phosphorylated to total ratio is significantly reduced due to large increases in total p65. RelB and p100 of the altNF-κB pathway were also increased; however, variation in

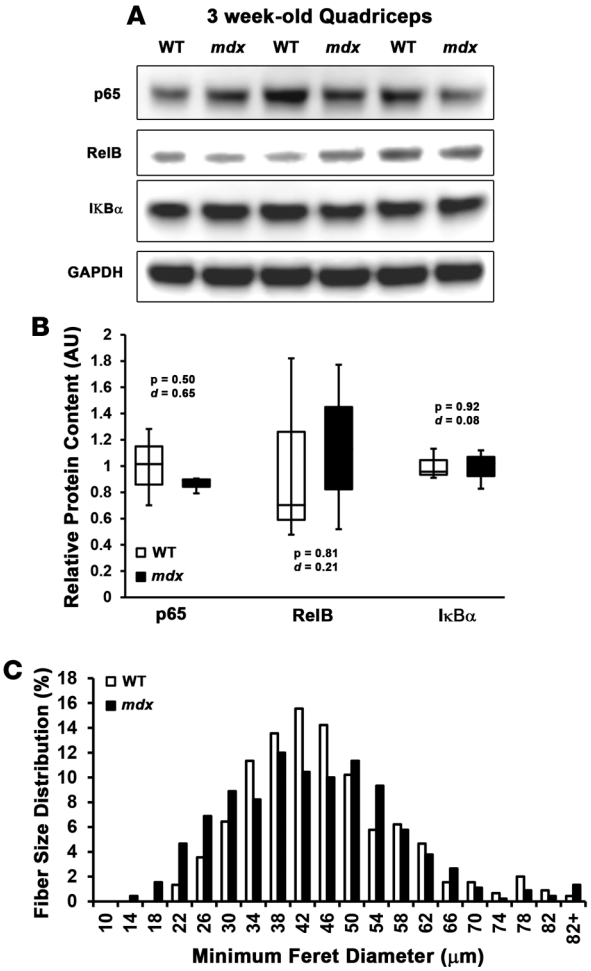

Figure 2. NF-κB is not elevated in predystrophic *mdx* muscle. (**A**) Representative immunoblot images and (**B**) related quantifications of 3-week-old WT (n = 3) and *mdx* (n = 3) quadriceps muscles for the NF-κB components p65, RelB, and IκBα. Protein levels were normalized to GAPDH signal and quantified relative to WT values. Data are displayed as box-and-whisker plots, indicating first and third quartiles, median, minimum, and maximum values, and were analyzed using 2-tailed Welch's t test with effect size displayed as Cohen's d. (**C**) Fiber size distribution in the quadriceps of 3-week-old WT and *mdx* mice, which is prior to the inflammatory degenerative stage of *mdx* pathology. Values are indicated as percentage of total muscle fiber population.

p52 content suggests that the formal activation of the alternate pathway (i.e., p100 processing) is not similarly increased (Figure 1C). Elevations of NF-κB, as well as the characteristic myofiber hypertrophy of *mdx* mice, were absent in 3-week-old *mdx* quadriceps (Figure 2, A–C), which is prior to the degenerative/inflammatory phase that occurs at 4 to 5 weeks of age in *mdx* mice. This indicates that total cellular NF-κB elevation is coincident with or subsequent to the severe degeneration and inflammation, and hence is not a direct consequence of dystrophin loss.

As PUFAs, such as docosahexaenoic acid (DHA) and eicosapentaenoic acid (EPA), and salicylic acid inhibit the activation of cNF-κB individually (15, 16), we evaluated the novel, orally bioavailable compounds edasalonexent and CAT-1041, which consist of either DHA or EPA, respectively, conjugated to salicylic acid (chemical structures shown in Figure 3A). This approach results in the accumulation and simultaneous intracellular release of 2 separate NF-κB inhibitors, leading to a more potent inhibition of NF-κB activity in RAW 246.7 (murine) macrophages stably expressing an NF-κB luciferase reporter than the components alone or in equimolar combination can achieve, as well as inhibition of LPS- and TNF-α–mediated p65 transcription in human peripheral blood mononuclear cells (Figure 3, B–D). Indeed, 5-month pilot trials of either edasalonexent or CAT-1041 in *mdx* mice resulted in improved resistance of extensor digitorum longus (EDL) muscles to eccentric damage (Figure 3E) with no apparent adverse effects. As edasalonexent, the DHA-conjugated compound, is in clinical development for the treatment of DMD (NCT02439216) and the 2 compounds demonstrated nearly identical in vitro and in vivo efficacy, we continued evaluation of the preclinical CAT-1041 compound for the treatment of dystrophinopathic muscle.

In a 6-month trial of CAT-1041 on individually housed *mdx* mice with ad libitum access to a voluntary running wheel, a model used to exacerbate the relatively mild dystrophic phenotype of *mdx* mice (18, 19), the CAT-1041 treatment group consistently ran greater distances than the untreated mice (Figure 4A), while body weight was not affected (Figure 4B). Treatment improved ex vivo function of the EDL and diaphragm (Figure 4C), and resulted in hypertrophy of the limb muscles, relative to the untreated group (Figure 4, D and E). Reductions in intramuscular fibrosis of the quadriceps, EDL, and diaphragm (Figure 5, A and B), and damage to the quadriceps, as visualized by sarcolemmal permeability to serum proteins (Figure 5, C and D), were evident with CAT-1041 treatment. Immunoblotting of quadriceps revealed that CAT-1041 reduced the expression of the NF-κB components p65, p105, p50, RelB, and p100, while p52 expression trended towards a reduction and the RelB/p65 ratio trended towards an increase (Figure 5E). In agreement with a decrease of the NF-κB system, lower levels of the inflammatory markers osteopontin, IL-6, IL-4, and MMP2, as well as the fibrosis markers FSP-1 and fibronectin were found (Figure 5F). CAT-1041 treatment in this cohort also resulted in reduced cardiac mass (Figure 6, A and B), fibrosis (Figure 6, C and D), and signaling of the Akt and ERK pathways (Figure 6, E and F), despite higher mouse activity, suggesting the potent skeletal muscle benefits do not exacerbate the *mdx* cardiomyopathy. Indeed, these results suggest that CAT-1041 actually improves the dystrophic heart phenotype. This is important, as cardiomyopathies in DMD are a leading cause of patient mortality (20).

While the benefits of canonical NF-κB inhibition on the dystrophic phenotype are likely multifaceted through reductions in inflammation (8), we were intrigued by the observed resilience to sarcolemma damage

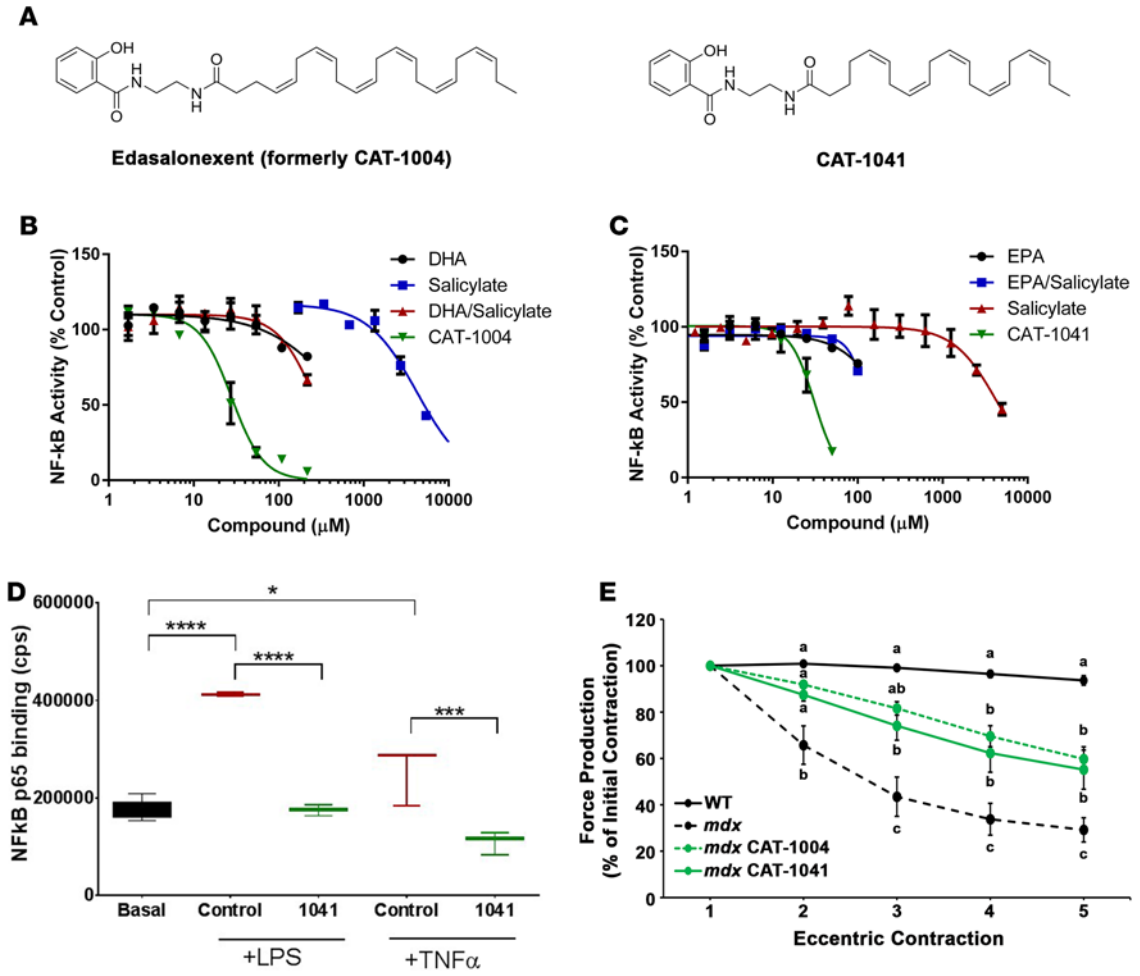

Figure 3. Edasalonexent and CAT-1041 are potent NF-κB inhibitors. (**A**) Chemical structures of edasalonexent (aka CAT-1004) and CAT-1041. (**B**) Edasalonexent and (**C**) CAT-1041 inhibit LPS-induced p65-dependent transcriptional activity in RAW 264 cells (mouse macrophage cell line). (**D**) CAT-1041 inhibits LPS- and TNF-α–stimulated p65 binding in human peripheral blood mononuclear cells. Data are displayed as box-and-whisker plots, indicating first and third quartiles, median, minimum, and maximum values. *$P < 0.05$, ***$P < 0.001$, ****$P < 0.0001$ for respective comparisons. (**E**) The treatment of *mdx* mice with either CAT-1041 or edasalonexent for 20 weeks results in reduced susceptibility of the extensor digitorum longus muscle to eccentric contraction–induced injury. Values are indicated as mean ± SEM; contraction-matched values not connected by a letter are significantly different by Tukey honest significant difference post-hoc test (α = 0.05).

by the treatment with these compounds (Figure 3F and Figure 5, C and D). Protein levels of utrophin, integrin α7, and integrin β1, stabilizers of dystrophin-deficient sarcolemma (21–23), were unchanged by CAT-1041 treatment (Figure 7, A and B). As shifts in cardiomyocyte NF-κB signaling towards RelB-mediated transcription causes upregulation of the membrane repair protein dysferlin (24), we sought to determine whether increases in dysferlin may be involved in the resiliency to damage by CAT-1041 treatment. Indeed, we found significant increases in full-length dysferlin protein, as detected with both Romeo (N-terminal) and Hamlet (C-terminal) monoclonal antibodies to dysferlin, in CAT-1041–treated quadriceps (Figure 7, C and D). The C72 C-terminal cleavage product (25, 26) was also increased with treatment, suggesting active membrane repair was enhanced in treated mice. While total *Dysf* gene expression was nearly 2-fold higher in treated mice (Figure 7E), expression of the canonical (calcium sensitive) C2A isoform of *Dysf* was significantly reduced. Instead, we found a nearly 14-fold increase in the expression of the C2A variant 1 (C2Av1), which is largely calcium insensitive and has a high affinity for phospholipids (27). A 40% increase in expression of *Dysf* containing exon 40a, which expresses the calpain-susceptible cleavage site to release the C72 fragment (25), was also found. In agreement with the increase in dysferlin C2Av1 expression, immunofluorescence shows greater intensity and homogeneity of dysferlin localization to the sarcolemma in CAT-1041–treated quadriceps (Figure 7F). These data suggest that a potentially novel component of cNF-κB inhibition by CAT-1041 involves an upregulation of dysferlin, possibly improving sarcolemma repair potential in the absence of dystrophin.

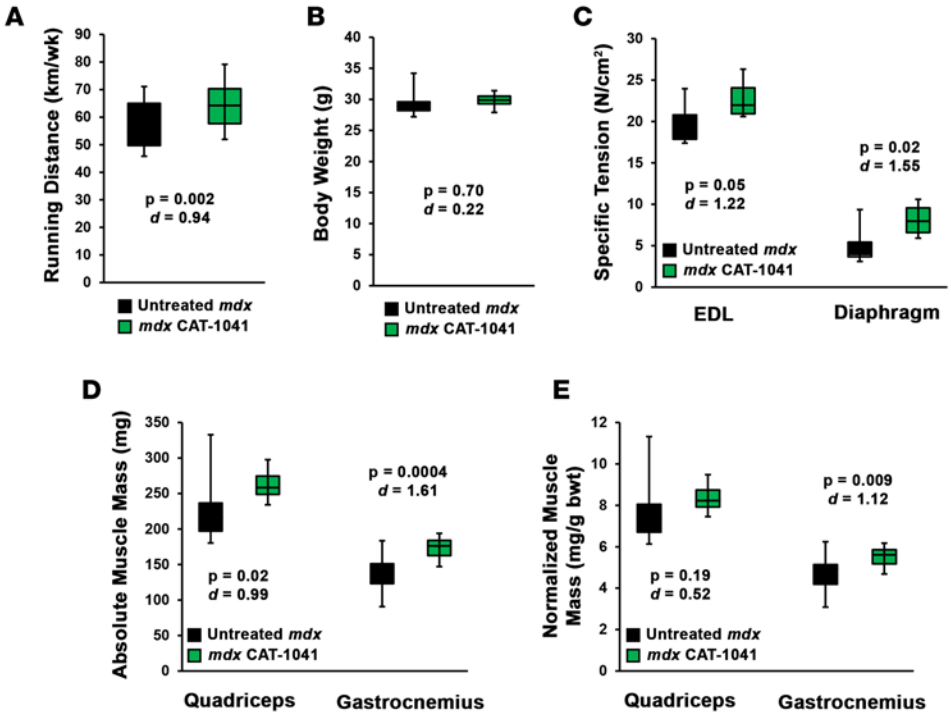

Figure 4. CAT-1041 treatment improves function of *mdx* mouse muscle. (**A**) Dystrophic *mdx* mice fed either control (n = 7) or CAT-1041–containing chow (n = 6) were provided in-cage voluntary running wheels for 25 weeks with daily distance monitoring. (**B**) Body weights, (**C**) ex vivo muscle function of the extensor digitorum longus (EDL) and diaphragm, and muscle masses of the quadriceps and gastrocnemius, reported as (**D**) absolute and (**E**) body weight–normalized masses, of untreated and CAT-1041–treated mice from this cohort. Data are displayed as box-and-whisker plots, indicating first and third quartiles, median, minimum, and maximum values, and were analyzed using 2-tailed Welch's t test with effect size displayed as Cohen's d.

Our group has previously reported dysferlin to be elevated in *mdx* muscle (28), so we further explored this observation in the context of localization and isoform expression. Immunofluorescent staining for dysferlin in *mdx* quadriceps revealed a heterogeneous localization pattern compared with WT muscle (Figure 8A), characterized by high levels of dysferlin abundance at the sarcolemma of small, regenerating fibers and low levels in many larger fibers. Gene expression of total *Dysf* and *Dysf* exon 40a were elevated in *mdx* (compared with WT) muscle; however, no difference exists in the C2A isoforms (Figure 8B). Thus, the increase in the C2Av1 isoform of dysferlin is not a normal phenomenon in *mdx* muscle, and its upregulation by CAT-1041 is unique and a potential modifier of the dystrophinopathic muscle phenotype.

CAT-1041's efficacy was also tested in the GRMD dog model of DMD, which better recapitulates pathology and progression of DMD patients than the *mdx* mouse. As a case study, an affected GRMD dog received daily oral CAT-1041 treatment for 9 months, starting at 3 months of age. Serial MRI measurements show that the treated dog exhibited substantially larger muscle volume of the anterior hind limb compartment (consisting of the tibialis cranialis [TC] and EDL muscles; outlined in Figure 9A), compared with age-matched untreated GRMD dogs, as soon as 2 months following treatment initiation (Figure 9B). In vivo ventilatory function testing revealed that at 12 months of age, the treatment end point, the CAT-1041 treatment results in larger tidal volume (Figure 9C) and better inspiratory compliance (Figure 9D), both indicators of improved diaphragm function, than untreated dogs. CAT-1041 also reduced histopathology in limb muscles, diaphragm, and heart (Figure 9E), decreased fibroblast prevalence in the TC and diaphragm (Figure 9F), improved homogeneity of diaphragm fiber size (Figure 9G), and increased homogeneity of sarcolemmal dysferlin in the diaphragm (Figure 9H). Thus, CAT-1041 has the potential to ameliorate the severe phenotype of GRMD muscle.

Discussion

DMD affects ~1 in 3,500 boys, and with potential cures, such as genetic and cellular therapies, still far away from widespread clinical use, a large focus of therapeutic development should be devoted towards therapies that can immediately benefit patients by slowing disease progression. Such therapies may have potential as monotherapies as well as adjunct therapies to complement genetic and/or cellular therapeutic approaches. The current report places the NF-κB inhibitors, edasalonexent and CAT-1041, into this category. These orally bioavailable conjugates of a PUFA and salicylic acid improve the severe dystrophic phenotype found in both mechanically damaged *mdx* mice and a GRMD dog, and create an environment that can support more successful muscle regeneration.

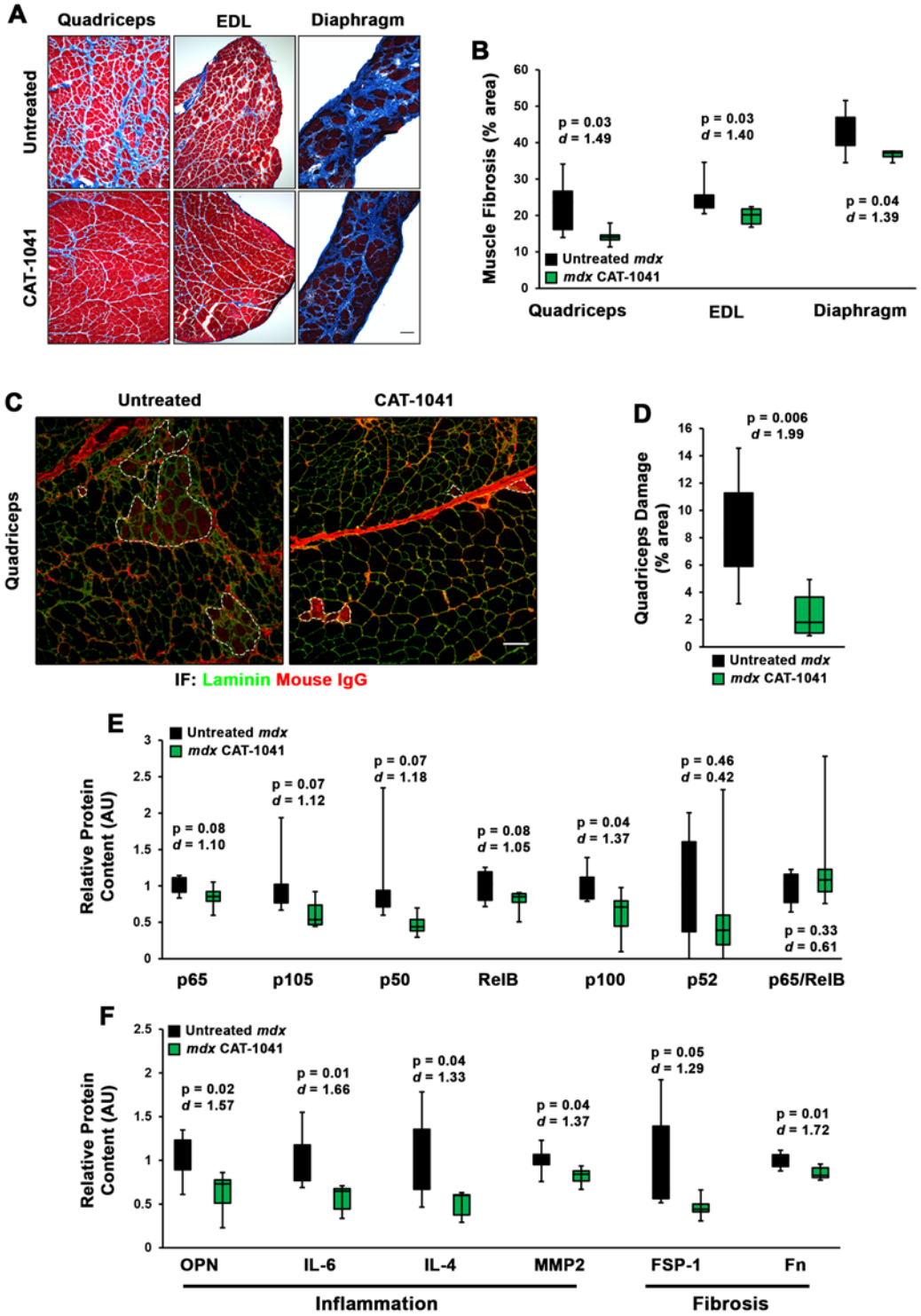

Figure 5. Phenotype of *mdx* muscle is improved by CAT-1041 treatment. Dystrophic *mdx* mice fed either control (n = 7) or CAT-1041–containing chow (n = 6) were provided in-cage voluntary running wheels for 25 weeks. (**A**) Representative images of Masson's trichrome staining and (**B**) accompanying quantification of intramuscular fibrosis of the quadriceps, extensor digitorum longus (EDL), and diaphragm as performed using 5 independent fields of view for each sample. (**C**) Muscle damage to the quadriceps was visualized by immunofluorescence (IF) staining muscle cross sections for laminin and endogenous mouse IgGs to label serum-permeable muscle fibers. The dotted lines demonstrate labeling of damaged fibers, which was (**D**) quantified as percentage of total area using 4 independent fields of view for each sample. Scale bars: 100 μm. Immunoblot quantifications for (**E**) NF-κB components and (**F**) markers of inflammation, including osteopontin (OPN), IL-6, IL-4, and matrix metalloproteinase (MMP) 2, and fibrosis, including fibroblast-specific protein 1 (FSP-1) and fibronectin (Fn), as measured by immunoblotting. Protein contents are normalized to Ponceau red–visualized loading. Data are displayed as box-and-whisker plots, indicating first and third quartiles, median, minimum, and maximum values, and were analyzed using 2-tailed Welch's t test with effect size displayed as Cohen's d.

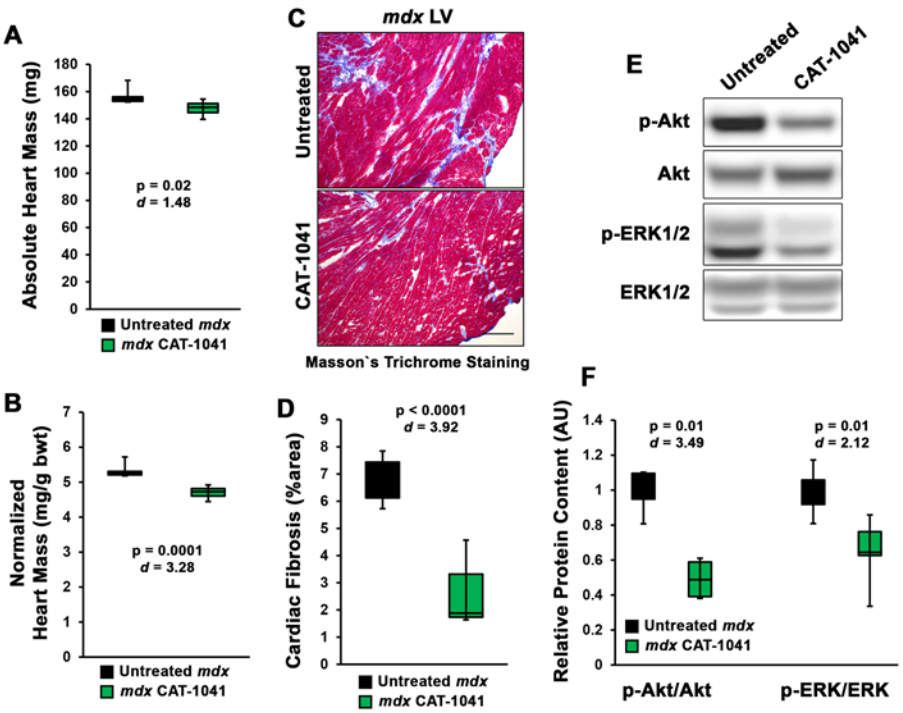

Figure 6. CAT-1041 improves cardiac phenotype of *mdx* mice. (**A**) Absolute and (**B**) body weight–normalized heart masses from *mdx* mice fed either control (n = 7) or CAT-1041–containing chow (n = 6) and provided in-cage voluntary running wheels for 25 weeks. (**C**) Representative Masson's trichrome staining images and (**D**) accompanying quantification of cardiac fibrosis of the left ventricle (LV) using 5 independent fields of view for each sample. Scale bar: 100 μm. (**E**) Representative immunoblots and (**F**) quantifications of the phosphorylation status of Akt and ERK1/2 in these hearts. Data are displayed as box-and-whisker plots, indicating first and third quartiles, median, minimum, and maximum values, and were analyzed using 2-tailed Welch's t test with effect size displayed as Cohen's d.

Canonical NF-κB inhibition has demonstrated great promise as a therapeutic target in dystrophin-deficient skeletal muscle. In particular, the work of Acharyya et al. provided evidence that cNF-κB is involved in *mdx* pathology by demonstrating that both p65 haploinsufficiency and administration of an NF-κB–inhibitory peptide (IKKγ/NEMO-binding domain; NBD) fused with a protein transduction domain (PTD; promotes cell entry) reduced the dystrophic phenotype of *mdx* mice (8). However, the translational limitations of this peptide-based approach were realized when long-term intravenous treatments with NBD provoked immune responses in GRMD dogs (29). An attractive feature of the compounds used in the current study is that they are orally bioavailable small molecules with low risk of toxicity that exhibit substantial NF-κB inhibitory effects and demonstrate the capacity to improve the dystrophic muscle phenotype in 2 animal models, with no signs of adverse events. In fact, a recently completed phase 1 trial with edasalonexent demonstrated high safety profiles in subjects after 2 weeks of administration (30), with plasma exposure levels that exceeded those observed in mice.

The beneficial effects of CAT-1041 on the dystrophic phenotype are likely multifaceted, as both inflammatory and fibrotic markers are reduced with long-term treatment in *mdx* mice (Figure 5). However, a surprising finding in this study was the significant increase in dysferlin content with CAT-1041, which coincides with a large increase in the gene expression of the C2Av1 splice variant of dysferlin. Taken together with the greater homogeneity of dysferlin staining at the sarcolemma, this suggests that CAT-1041 may protect dystrophic muscle from damage by upregulating a dysferlin variant that constitutively resides near the sarcolemma despite elevated intracellular Ca^{2+} concentrations. As muscle-specific transgenic overexpression of (presumably canonical) dysferlin fails to improve the muscle phenotype of *Scgd*$^{-/-}$ mice (31) and actually causes a myopathy at very high levels (32), the specific induction of the C2Av1 isoform appears to be key for this hypothesized protective effect in the model utilized in the current study. This warrants further investigation of the C2Av1 dysferlin variant as a potential modifier of mechanical muscle damage, which may be additive to other sarcolemma-stabilizing strategies, such as dystrophin replacement or utrophin overexpression.

In addition to the robust skeletal muscle benefit of CAT-1041 treatment, this compound appears to protect the *mdx* hearts from cardiac pathology, as cardiac hypertrophy, fibrosis, and associated signaling pathways were reduced with treatment. The reduction in cardiac fibrosis was also found in the treated GRMD dog heart. Unfortunately, cardiac function was not evaluated in this study, as the terminal time points selected for skeletal muscle phenotype were earlier than the typical age of cardiomyopathy onset in both *mdx* and GRMD models (discussed in ref. 33). Future studies focused on cardiac function are

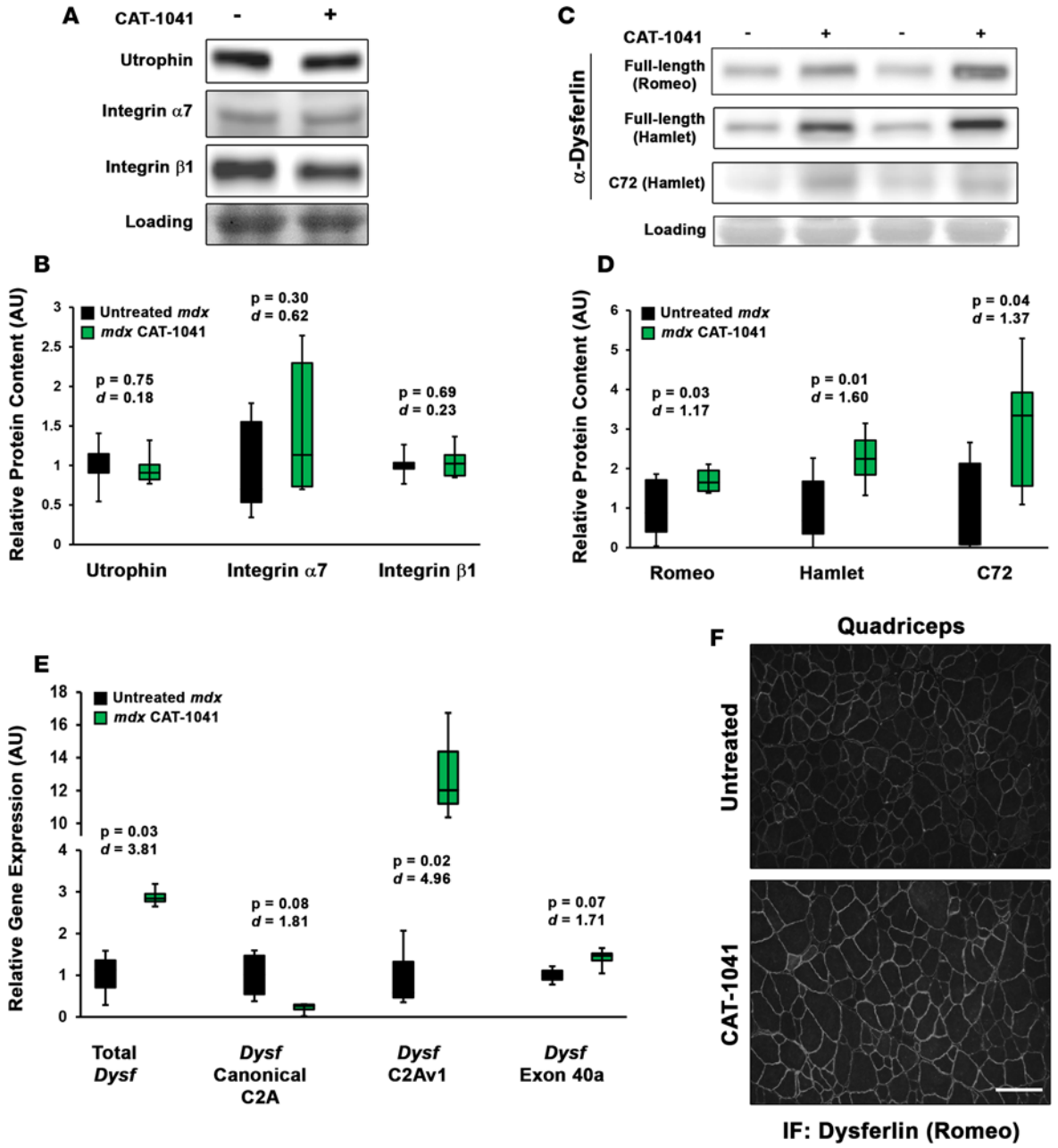

Figure 7. Dysferlin content is increased in CAT-1041–treated *mdx* mice. (**A**) Representative immunoblots and (**B**) quantifications of utrophin, integrin α7, and integrin β1 in the quadriceps lysates from *mdx* mice fed either control (n = 7) or CAT-1041–containing chow (n = 6) and provided in-cage voluntary running wheels for 25 weeks. (**C**) Representative immunoblots and (**D**) quantifications of full-length dysferlin, as detected with both Romeo (N-terminal) and Hamlet (C-terminal) antibodies, and the C72 dysferlin cleavage product, as detected with Hamlet antibody. Protein contents are normalized to Ponceau red–visualized loading. Gene expression of total *Dysf* and isoforms containing the canonical C2A isoform, C2A variant 1 (C2Av1), and exon 40a in the quadriceps of untreated (n = 4) and CAT-1041–treated (n = 4) *mdx* mice, using *Gapdh* as the ΔΔCt normalization gene. (**F**) Immunofluorescence (IF) staining for N-terminal dysferlin in stabilized regions of untreated and CAT-1041–treated quadriceps cross sections acquired under identical conditions. Scale bar: 100 μm. Data are displayed as box-and-whisker plots, indicating first and third quartiles, median, minimum, and maximum values, and were analyzed using 2-tailed Welch's t test with effect size displayed as Cohen's d.

needed to determine if treatment with CAT-1041 or edasalonexent prevents or slows the onset of functional cardiomyopathy in our models of DMD.

In summary, the data reported in the current study demonstrate that a new class of orally bioavailable NF-κB inhibitors improves the phenotype of dystrophic muscles. These data suggest that edasalonexent is potentially a treatment option to improve both quantity and quality of DMD patient muscles.

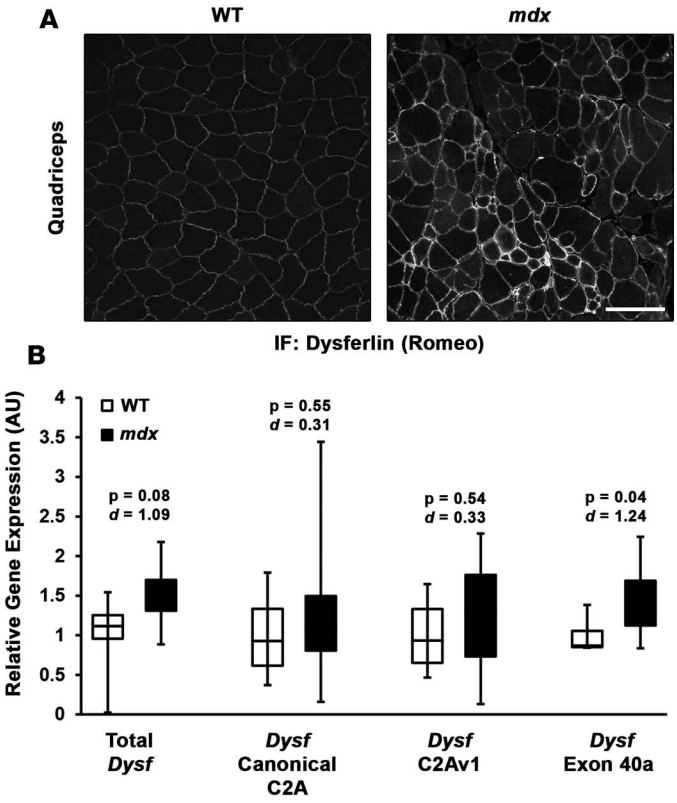

Figure 8. Dysferlin content is modified in sedentary *mdx* muscle. (**A**) Immunofluorescence (IF) staining for N-terminal dysferlin with Romeo antibody in 12-week-old WT and *mdx* quadriceps cross sections acquired under identical conditions. Scale bar: 100 μm. (**B**) Gene expression of *Dysf* variants in WT (n = 6) and *mdx* (n = 8) quadriceps, using *Gapdh* as the ΔΔCt normalization gene. Data are displayed as box-and-whisker plots, indicating first and third quartiles, median, minimum, and maximum values, and were analyzed using 2-tailed Welch's t test with effect size displayed as Cohen's d.

Methods

Mice. The experimental procedures used in this study were approved by the University of Pennsylvania IACUC using male *mdx* or WT mice on the C57BL/10 background. Drug treatment protocols entailed feeding individually housed mice a specialty control chow or chow containing either CAT-1041 or edasalonexent (0.75% w/w) ad libitum starting at 4 weeks of age. Average drug consumption typically ranged between 0.75 and 1 mg/g body weight per day. The 24-hour plasma exposures at this dosage were 450 and 270 ng hr/ml for edasalonexent and CAT-1041, respectively. These values are at the lower end of clinical exposures observed in phase 1 studies in adults and boys with DMD (30), suggesting that efficacy is obtained in the *mdx* mouse at clinically relevant exposures. Moreover, the exposure of edasalonexent was 7.2-fold greater in the gastrocnemius muscle compared with plasma and 4.0-fold higher in muscle than plasma for CAT-1041, demonstrating that both molecules are able to effectively reach and accumulate in skeletal muscle. In running wheel arms of this study, mice were provided ad libitum access to running wheels (11-cm diameter) for 25 weeks beginning at 6 weeks of age, with revolution counts and body weights monitored daily.

NF-κB reporter assay. RAW 264.7 macrophages stably transfected with 3xNF-κB-luciferase reporter were the gift of Steve Shoelson (Joslin Diabetes Center, Boston, Massachusetts, USA). One day prior to the assay, cells were scraped from 75-cm^2 tissue culture flasks and seeded onto 96-well plates at a density of 30,000 cells per well. Edasalonexent, CAT-1041, EPA, and the combination of both EPA and salicylate were prepared as 100 mM stocks in ethanol, which were then diluted 1:100 into FBS. These 1 mM FBS stocks were then serially diluted 1:2 in FBS supplemented with 1% ethanol, and all dilutions were sonicated for 30 minutes. Medium from the 96-well plate was aspirated and replaced with 90 μl sera-free DMEM. To these cells, 10 μl of FBS/compound dilutions were added to the wells, in triplicate, to create a dilution series ranging from 100 μM to 0.78 μM in 10% FBS/0.1% ethanol. In the case of salicylate only, a stock solution of 10 mM sodium salicylate was made in DMEM containing 10% FBS/0.1% ethanol by directly dissolving sodium salicylate powder into the medium. This solution was serially diluted 1:2 in DMEM/10%FBS/0.1% ethanol. Medium from the 96-well plate was aspirated, and 100 μl of DMEM/10% FBS/0.1% ethanol/salicylate dilutions were added. Cells were incubated at 37°C for 3 hours before stimulation with 5 μl of 4 μg/ml LPS (Sigma-Aldrich, L2630) in AlamarBlue viability reagent (Invitrogen, DAL1100) or 5 μl AlamarBlue only for unstimulated control cells. Cells were then incubated at 37°C for an additional 2 hours. Cell viability was assessed using a Victor X5 plate reader (PerkinElmer), measuring fluorescence with an excitation filter of 550 nm and an emission filter of 590 nm. Wells were then aspirated, and 100 μl Brite Lite Plus luciferase reagent (PerkinElmer, 6016761) was added to each well. Luminescence was measured using the Victor X5 plate reader. Data are presented as percentage of LPS-stimulated control, calculated as 100 × (CPS sample – average CPS unstimulated control)/(average CPS LPS stimulated control – average CPS unstimulated control), where CPS is counts per second. Error bars represent standard error of the mean (SEM) for experiments performed in triplicate.

p65 DNA-binding ELISA. Human peripheral blood mononuclear cells (PBMCs) were collected from healthy donor blood, collected in EDTA collection tubes, using Ficoll-Paque PLUS according to the manufacturer's protocol (Sigma-Aldrich, GE17-1440-02). Collected cells were washed 2 times in RPMI medium,

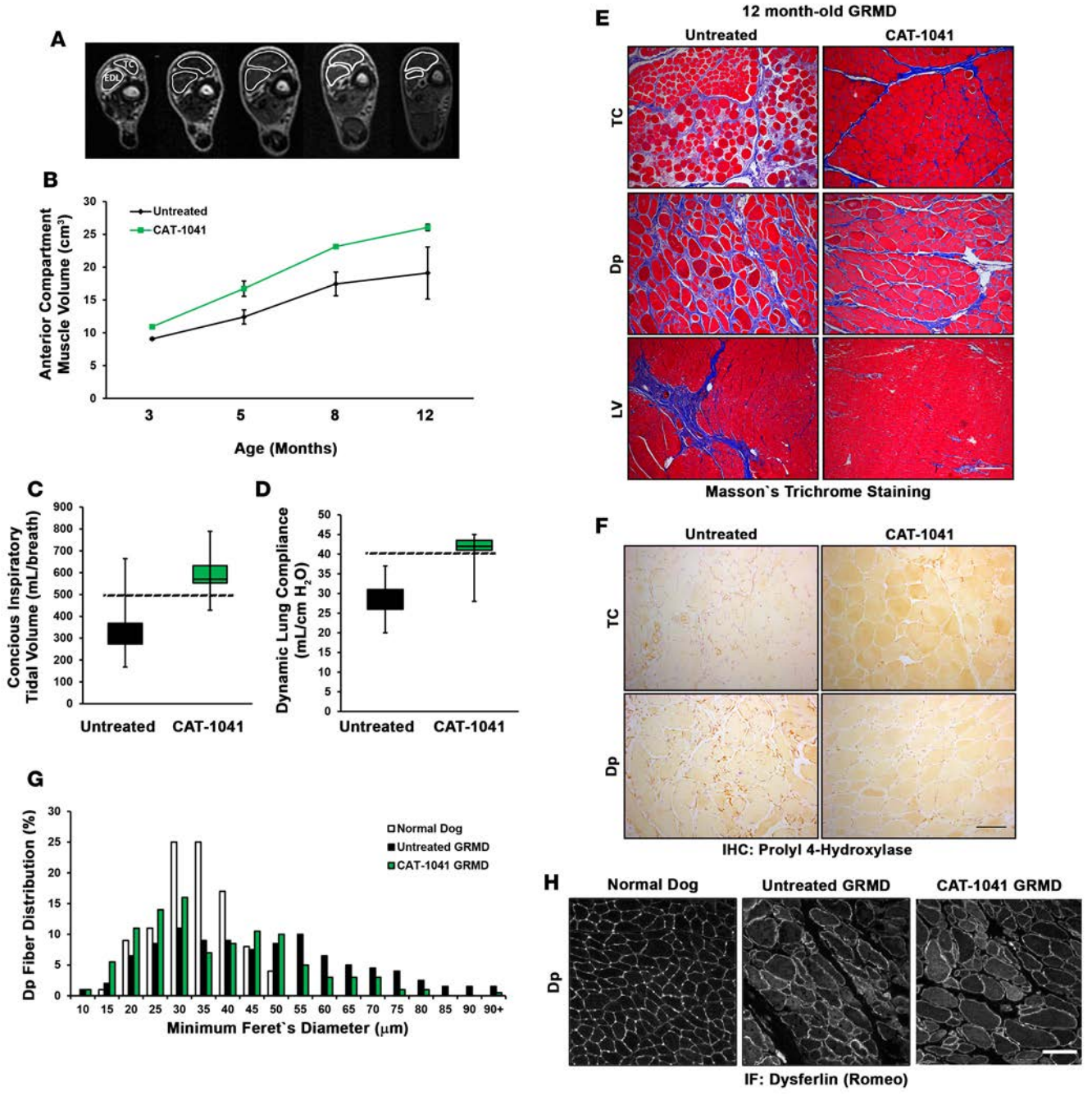

Figure 9. GRMD phenotype is improved by CAT-1041 in a canine case study. An affected golden retriever muscular dystrophy (GRMD) dog was treated with CAT-1041 daily, starting at 3 months of age, for 9 months. (**A**) Serial magnetic resonance imaging (MRI) to measure the (**B**) muscle volume of the anterior compartment of the hind limb (consisting of the tibialis cranialis [TC] and extensor digitorum longus [EDL] muscles) in the treated and age-matched, untreated GRMD dogs (n = 3). At the end of the 9-month treatment protocol, the dogs were evaluated for ventilatory function, as measured by (**C**) conscious inspiratory tidal volume and (**D**) dynamic lung compliance (20 breaths per dog). Dotted lines indicate minimum reference values for size-matched normal dogs. (**E**) Representative Masson's trichrome staining of untreated and CAT-1041–treated TC, diaphragm (Dp), and left ventricle (LV). (**F**) Immunohistochemical (IHC) staining of the fibroblast marker prolyl 4-hydroxylase in the TC and Dp. (**G**) Dp fiber size distribution and (**H**) N-terminal dysferlin immunofluorescence (IF) of normal, untreated GRMD, and CAT-1041–treated GRMD dogs. Scale bars: 100 μm. Data are displayed as (**B**) mean ± SD of left and right limbs, (**C** and **D**) box-and-whisker plots, indicating first and third quartiles, median, minimum, and maximum values of total breaths measured, or (**G**) percentage total muscle fiber population (n = 200–400 fibers per sample).

counted using a hemacytometer, and brought up to a density of 1×10^6 cells/ml. Cells (1 ml) were then proportioned into each well of a 24-well plate. For compound treatment, CAT-1041 was solubilized in 100% ethanol to generate a 50 mM stock solution. This stock solution was then diluted 1:100 into FBS and sonicated for 30 minutes (along with a matched FBS control containing 1% ethanol). FBS/ethanol and the FBS/CAT-1041 mixtures were then diluted 1:10 over the PBMCs such that the final concentrations were 0.1% ethanol/10% FBS ± 50 μM CAT-1041. Control- and CAT-1041–treated cells were incubated at 37°C in a humidified CO_2 incubator for 2 hours before stimulating with either 250 ng/ml final LPS or 20 ng/ml TNF-α for 1 hour. Cells were then washed 2 times in PBS and lysed in Passive Lysis Buffer (Promega, E194). Lysate (10 μl) was then used for chemiluminescent p65 DNA-binding ELISA following the manufacturer's protocol (Thermo Scientific, 89859). A Bradford assay was then performed on the remaining lysates to quantify protein. Data are expressed as normalized CPS divided by total protein (in μg). Error bars represent standard deviation (SD) of experiments performed in triplicate.

Muscle mechanics. Maximal tetanic tension and eccentric damage assessments of the EDL and diaphragm were evaluated as previously described (34) by the Muscle Physiology Core at the University of Pennsylvania. Briefly, the muscles of anesthetized mice were dissected and placed in physiological Ringer's solution gas equilibrated with 95% O_2/5% CO_2. After determining optimal length, muscles were subjected to 3 isometric contractions (stimulated at 120 Hz for 500 ms) to determine maximal tetanic tension (Po). Subsequently, a series of 5 eccentric contractions with (stimulated at 80 Hz for 700 ms) a stretch of 10% optimal length was imposed on the muscle in the last 200 ms of each contraction. Each contraction was separated by a 5-minute rest period. Following experimental procedures, muscles were weighed, frozen embedded in OCT or snap-frozen, and stored at –80°C until further use. Force measurements and dissections were performed by investigators blind to treatment groups.

Histology, immunofluorescence, and immunohistochemistry. OCT- or paraffin-embedded samples were sectioned and stained with Masson's trichrome (Polysciences, Inc.). Slides were viewed using a Leitz DMRBE microscope (Leica) and imaged with a Leica DCF480 digital camera. Fibrosis was quantified using k-means segmentation in ImageJ software (NIH) by investigators blind to treatment groups.

For immunofluorescence, frozen, OCT-embedded samples were sectioned at 10 μm, fixed in ice-cold acetone, blocked in 5% BSA-PBS, and incubated with anti-dysferlin (Romeo Rb mAb; Abcam; catalog ab124684), and/or anti-laminin (Acris, catalog BM6046P) primary antibodies overnight at 4°C. Following PBS washes, slides were incubated in donkey anti–rabbit Alexa-568 (catalog A10042), donkey anti–rat Alexa-488 (catalog A-21208), and/or donkey anti–mouse Alexa-568 (catalog A10037) secondary antibodies (all Life Technologies), washed with PBS, coverslipped with VectaShield (Vector Labs), and imaged using a Leitz DMRBE microscope with a Leica DCF480 digital camera. Lipofuscin-dependent autofluorescence was eliminated from sections using 1% Sudan black B dissolved in 70% ethanol following secondary antibody incubation. Comparative images were stained, acquired, and processed under identical conditions. Quantifications were performed using ImageJ software on multiple images per sample.

For immunohistochemistry, paraffin-embedded samples were sectioned at 5 μm, deparaffinized, antigen-retrieved in heated 1 mM citrate buffer (pH 6), treated for endogenous peroxidase activity, blocked with 5% goat serum, and incubated with anti–prolyl 4-hydroxylase (Proteintech, catalog 11245-1-AP) primary antibody for 1 hour at room temperature. Following PBS washes, sections were blocked with avidin/biotin (Biocare), incubated with goat anti–rabbit biotinylated secondary antibody (Vector Labs, catalog BA-1000), washed, and incubated with HRP-conjugated streptavidin (Vector Labs). Sections were developed with DAB reagent (Dako), counterstained with hematoxylin (Dako), coverslipped, and imaged using a Leitz DMRBE microscope with a Leica DCF480 digital camera.

Immunoblotting. Snap-frozen samples were finely crushed and homogenized in T-PER buffer (Thermo Scientific) supplemented with protease and phosphatase inhibitors (Thermo Scientific). Protein concentration of resulting supernatant was determined using Bio-Rad Protein Assay (Bio-Rad). Protein samples were boiled in 4× sample buffer, resolved by SDS-PAGE using 4%–12% SDS-polyacrylamide gels (Life Technologies), and transferred to nitrocellulose membranes using the iBlot system (Life Technologies). Membranes were blocked in 5% milk-TBST and incubated with primary antibody overnight at 4°C. Following TBST washes, membranes were incubated in the appropriate HRP-congugated secondary antibody for 1 hour at room temperature, washed, incubated for 5 minutes in ECL reagent (Thermo Scientific), and imaged using the LI-COR C-DiGit (LI-COR Biosciences) imaging system. Primary antibodies used in this study include: p65 (catalog 4764), p-p65 (Ser536, catalog 3033), RelB (catalog 4922), IκBα (catalog

4814), p100/52 (catalog 4882), p-Akt (Ser473, catalog 9271), Akt (catalog 9272), p-ERK1/2 (Thr202/204, catalog 9101), ERK1/2 (catalog 9102) (all Cell Signalling Technology); p105/50 (catalog ab7971), IL-6 (catalog ab83339), IL-4 (catalog ab9728), FSP/S100A4 (catalog ab27957), Romeo dysferlin N-terminal Rb mAb, (catalog ab124684), Hamlet C-terminal Ms mAb (catalog 139379), integrin β1 (catalog ab179471) (all Abcam); osteopontin (R&D Systems, catalog AF808); MMP2 (Novus, catalog NB200-193); fibronectin (Sigma-Aldrich, catalog F3648); utrophin (Vector Labs, catalog VP-U579); and integrin α7 (Abnova, catalog H00003679-M01). Blots for phosphorylated proteins were stripped and reprobed for total protein. Membranes underwent a final reprobing with GAPDH (Santa Cruz Biotechnology, catalog sc-25778) and/or were stained with Ponceau red and imaged for loading normalization. Band signal intensities were measured using Image Studio Lite software (LI-COR Biosciences), normalized to sample loading, and reported relative to respective control samples.

Real-time PCR. RNA was isolated from finely crushed snap-frozen mouse quadriceps samples using TRIzol Reagent (Life Technologies), treated with DNAse (Promega), and reverse transcribed using the SuperScript III kit (Life Technologies). Resulting cDNA was analyzed by real-time PCR using RQG SYBR Green supermix (Qiagen) in a Rotor Gene Q real-time PCR machine (Qiagen). The following mouse-specific *Dysf* primers were used: total (forward) 5′-GCCCCGGGGAAGATGTGCTGATT-3′ and (reverse) 5′-CATTGGGGTCCTTGGGCTGTAA-3′; canonical C2A isoform (forward) 5′-TGCTGCGAGTCTTCATCCTTTTT-3′ and (reverse) 5′-AACCTGTTTCTTCCCATCGTCTCA-3′; C2A variant 1 (forward) 5′-AGCAACCTCCCCAATGTGAAGAAG-3′ and (reverse) 5′-CTGGGGGTGGCGTGTAGGAC-3′; exon 40a (forward) 5′-CACGCCTGCCTTCTTCCTG-3′ and (reverse) 5′-GTCTGCCCACCACACTCCAC-3′. Primers for *Gapdh* (forward) 5′-AGCAGGCATCTGAGGGCCCA-3′ and (reverse) 5′-TGTTGGGGGCCGAGTTGGGA-3′ were used for ΔΔCt normalization.

GRMD study. Three-month-old GRMD dogs were administered either control or CAT-1041 (250 mg/kg/day) via oral gavage daily for 9 months. At final endpoints, dogs were euthanized, and harvested samples were fixed in 10% formalin or frozen embedded in OCT for histological evaluation. All animals were handled in compliance with NIH and institutional guidelines that were approved by the IACUC of the University of Pennsylvania.

MRI. Three-dimensional (3D) gradient echo (TR, 19.2 ms; TE, 2.3 ms; flip angle, 30; NEX, 3; slices, 86; slice thickness, 2 mm) images of the lower hind limbs were acquired using a 1.5T GE scanner with a wrist volume coil. Each hind limb was imaged separately, and the positioning of the coil enabled the entire anterior compartment (AC) of the lower hind limb to be imaged. The AC included the TA and EDL muscles. During the scanning protocol, dogs were induced with a continuous rate of infusion of propofol (1.0–2.0 mg/min/kg) and fentanyl (0.005 mg/kg/min), with maintenance via propofol (0.2 mg/kg/min), fentanyl (0.7 μg/kg/min), and a bolus of cisatracurium (0.1 mg/kg). Respiration, electrocardiogram, O_2 saturation, and blood pressure were monitored during the imaging procedures. For the MRI analysis, the size of the AC of the lower hind limbs was measured using OsiriX software (v.6.5.2).

GRMD lung function. A 20-gauge, 48-mm catheter was placed in the right cephalic vein in each dog. The dogs were placed in sternal recumbency on a table. A face mask with a tight-fitting rubber diaphragm was placed over each dog's muzzle and attached to the sensor of a CO_2SMO mainstream capnograph/pulse oximeter. Once the dogs had calmed and were breathing room air normally, inspiratory and expiratory tidal volume, peak inspiratory and expiratory flow rates, and end-tidal carbon dioxide ($EtCO_2$) were collected over 20 spontaneous, awake breaths for each dog.

Following collection of these respiratory variables, general anesthesia was induced with propofol (10 mg/ml) administered via slow intravenous injection. Each dog was intubated with an appropriately sized endotracheal tube and administered 100% oxygen via a Bain anesthesia circuit with the oxygen flow set at 60 to 100 ml/kg/min. General anesthesia was maintained with propofol (2.5 to 5 mg/kg slow intravenous injection) as needed during the procedure. Inhalant anesthetic was not used.

With the dogs still in sternal recumbency, intermittent positive pressure ventilation was performed using a 2-liter rebreathing bag to manually administer positive pressure breaths at a respiratory rate of 15 to 20 breaths per minute, with a peak airway pressure of 12 to 15 cmH_2O and an inspiratory time of 1 to 1.5 seconds per breath. Inspiratory and expiratory tidal volume, peak inspiratory and expiratory flow rates, $EtCO_2$, dynamic compliance (Cdyn), and inspiratory and expiratory airway resistance were measured using the CO_2SMO. Variables were collected over 20 consecutive, manually administered breaths. Following this data collection, the dogs were allowed to breathe spontaneously while intubated and con-

nected to the CO_2SMO. Inspiratory and expiratory tidal volumes and peak inspiratory and expiratory flow rates were collected over 20 spontaneous breaths. Following all data collection, the dogs were extubated and recovered uneventfully.

Statistics. Two-tailed Welch's *t* test (effect size displayed as Cohen's *d*) and 1-way ANOVA (Tukey honest significant difference post-hoc tests) were used to analyze data, where appropriate ($P < 0.05$ is considered significant). Values are represented as mean ± SEM, mean ± SD, or box-and-whisker plots of the 5 statistical summary (first and third quartiles, median, minimum, and maximum), where indicated.

Study approval. All animal procedures were approved by the IACUC of the University of Pennsylvania.

Author contributions

Research and study design was contributed by DWH, MMS, MRJ, GAW, and HLS. DWH, MMS, SCF, CCC, MZ, and GAW conducted experimental procedures and data acquisition. All authors were involved in data analysis, interpretation, and manuscript writing.

Acknowledgments

This work was funded by a Wellstone Muscular Dystrophy Cooperative Center grant (U54-AR-052646) from the NIH to HLS, a Parent Project Muscular Dystrophy grant to HLS, and support from the MDA to Catabasis Pharmaceuticals. We also acknowledge the support from grants from the MDA (grant 175552) to SCF and NIH (R01AR056973) to GAW. DWH was supported on the T32 training grant to the Pennsylvania Muscle Institute (T32-AR053461) for part of this work. We acknowledge the technical assistance of Patricia O'Donnell, Tracey Sikora, and Therese Ruanethe of the University of Pennsylvania veterinary staff, Min Liu and Zuozhen Tian of the University of Pennsylvania Muscle Physiology Core, Jen Pham, Pedro Acosta, Diana Menendez, Klara Pendrak, Alexandra Agathis, Chris Phillips, Adam George, and Jannik Arbogast.

Address correspondence to: H. Lee Sweeney, 1200 Newell Drive, ARB R5-216, Gainesville, Florida 32610-0267, USA. Phone: 352.273.9416; E-mail: lsweeney@ufl.edu.

1. Hoffman EP, Brown RH, Kunkel LM. Dystrophin: the protein product of the Duchenne muscular dystrophy locus. *Cell*. 1987;51(6):919–928.
2. Petrof BJ, Shrager JB, Stedman HH, Kelly AM, Sweeney HL. Dystrophin protects the sarcolemma from stresses developed during muscle contraction. *Proc Natl Acad Sci U S A*. 1993;90(8):3710–3714.
3. Bakkar N, Guttridge DC. NF-kappaB signaling: a tale of two pathways in skeletal myogenesis. *Physiol Rev*. 2010;90(2):495–511.
4. Marienfeld R, May MJ, Berberich I, Serfling E, Ghosh S, Neumann M. RelB forms transcriptionally inactive complexes with RelA/p65. *J Biol Chem*. 2003;278(22):19852–19860.
5. Legarda-Addison D, Ting AT. Negative regulation of TCR signaling by NF-kappaB2/p100. *J Immunol*. 2007;178(12):7767–7778.
6. Sasaki CY, Barberi TJ, Ghosh P, Longo DL. Phosphorylation of RelA/p65 on serine 536 defines an I{kappa}B{alpha}-independent NF-{kappa}B pathway. *J Biol Chem*. 2005;280(41):34538–34547.
7. Pradère JP, Hernandez C, Koppe C, Friedman RA, Luedde T, Schwabe RF. Negative regulation of NF-κB p65 activity by serine 536 phosphorylation. *Sci Signal*. 2016;9(442):ra85.
8. Acharyya S, et al. Interplay of IKK/NF-kappaB signaling in macrophages and myofibers promotes muscle degeneration in Duchenne muscular dystrophy. *J Clin Invest*. 2007;117(4):889–901.
9. Singh R, et al. Increases in nuclear p65 activation in dystrophic skeletal muscle are secondary to increases in the cellular expression of p65 and are not solely produced by increases in IkappaB-alpha kinase activity. *J Neurol Sci*. 2009;285(1–2):159–171.
10. Messina S, et al. Activation of NF-kappaB pathway in Duchenne muscular dystrophy: relation to age. *Acta Myol*. 2011;30(1):16–23.
11. Monici MC, Aguennouz M, Mazzeo A, Messina C, Vita G. Activation of nuclear factor-kappaB in inflammatory myopathies and Duchenne muscular dystrophy. *Neurology*. 2003;60(6):993–997.
12. Tang Y, et al. Inhibition of the IKK/NF-κB pathway by AAV gene transfer improves muscle regeneration in older mdx mice. *Gene Ther*. 2010;17(12):1476–1483.
13. Delfin DA, Xu Y, Peterson JM, Guttridge DC, Rafael-Fortney JA, Janssen PM. Improvement of cardiac contractile function by peptide-based inhibition of NF-κB in the utrophin/dystrophin-deficient murine model of muscular dystrophy. *J Transl Med*. 2011;9:68.
14. Peterson JM, et al. Peptide-based inhibition of NF-κB rescues diaphragm muscle contractile dysfunction in a murine model of Duchenne muscular dystrophy. *Mol Med*. 2011;17(5–6):508–515.
15. Kopp E, Ghosh S. Inhibition of NF-kappa B by sodium salicylate and aspirin. *Science*. 1994;265(5174):956–959.
16. Zwart SR, Pierson D, Mehta S, Gonda S, Smith SM. Capacity of omega-3 fatty acids or eicosapentaenoic acid to counteract weightlessness-induced bone loss by inhibiting NF-kappaB activation: from cells to bed rest to astronauts. *J Bone Miner Res*. 2010;25(5):1049–1057.
17. Vu CB, et al. Synthesis and characterization of fatty acid conjugates of niacin and salicylic acid. *J Med Chem*. 2016;59(3):1217–1231.

18. De Luca A, et al. Gentamicin treatment in exercised mdx mice: Identification of dystrophin-sensitive pathways and evaluation of efficacy in work-loaded dystrophic muscle. *Neurobiol Dis*. 2008;32(2):243–253.
19. Smythe GM, White JD. Voluntary wheel running in dystrophin-deficient (mdx) mice: Relationships between exercise parameters and exacerbation of the dystrophic phenotype. *PLoS Curr*. 2011;3:RRN1295.
20. Bushby K, Muntoni F, Bourke JP. 107th ENMC international workshop: the management of cardiac involvement in muscular dystrophy and myotonic dystrophy. 7th-9th June 2002, Naarden, the Netherlands. *Neuromuscul Disord*. 2003;13(2):166–172.
21. Burkin DJ, Wallace GQ, Nicol KJ, Kaufman DJ, Kaufman SJ. Enhanced expression of the alpha 7 beta 1 integrin reduces muscular dystrophy and restores viability in dystrophic mice. *J Cell Biol*. 2001;152(6):1207–1218.
22. Heller KN, Montgomery CL, Janssen PM, Clark KR, Mendell JR, Rodino-Klapac LR. AAV-mediated overexpression of human α7 integrin leads to histological and functional improvement in dystrophic mice. *Mol Ther*. 2013;21(3):520–525.
23. Tinsley JM, Potter AC, Phelps SR, Fisher R, Trickett JI, Davies KE. Amelioration of the dystrophic phenotype of mdx mice using a truncated utrophin transgene. *Nature*. 1996;384(6607):349–353.
24. Tzeng HP, et al. Dysferlin mediates the cytoprotective effects of TRAF2 following myocardial ischemia reperfusion injury. *J Am Heart Assoc*. 2014;3(1):e000662.
25. Redpath GM, et al. Calpain cleavage within dysferlin exon 40a releases a synaptotagmin-like module for membrane repair. *Mol Biol Cell*. 2014;25(19):3037–3048.
26. Waddell LB, et al. Dysferlin, annexin A1, and mitsugumin 53 are upregulated in muscular dystrophy and localize to longitudinal tubules of the T-system with stretch. *J Neuropathol Exp Neurol*. 2011;70(4):302–313.
27. Fuson K, et al. Alternate splicing of dysferlin C2A confers Ca^{2+}-dependent and Ca^{2+}-independent binding for membrane repair. *Structure*. 2014;22(1):104–115.
28. Barton ER, Wang BJ, Brisson BK, Sweeney HL. Diaphragm displays early and progressive functional deficits in dysferlin-deficient mice. *Muscle Nerve*. 2010;42(1):22–29.
29. Kornegay JN, et al. NBD delivery improves the disease phenotype of the golden retriever model of Duchenne muscular dystrophy. *Skelet Muscle*. 2014;4:18.
30. Donovan JM, Zimmer M, Offman E, Grant T, Jirousek MR. A novel NF-κB inhibitor (edasalonexent, CAT-1004) in development as a disease-modifying treatment for patients with Duchenne muscular dystrophy: phase 1 safety, pharmacokinetics, and pharmacodynamics in adult subjects. *J Clin Pharmacol*. In Press.
31. Millay DP, et al. Genetic manipulation of dysferlin expression in skeletal muscle: novel insights into muscular dystrophy. *Am J Pathol*. 2009;175(5):1817–1823.
32. Glover LE, et al. Dysferlin overexpression in skeletal muscle produces a progressive myopathy. *Ann Neurol*. 2010;67(3):384–393.
33. Hammers DW, Sleeper MM, Forbes SC, Shima A, Walter GA, Sweeney HL. Tadalafil treatment delays the onset of cardiomyopathy in dystrophin-deficient hearts. *J Am Heart Assoc*. 2016;5(8):8.
34. Morine KJ, Bish LT, Pendrak K, Sleeper MM, Barton ER, Sweeney HL. Systemic myostatin inhibition via liver-targeted gene transfer in normal and dystrophic mice. *PLoS One*. 2010;5(2):e9176.